Improved Air Quality Forecasting
Invest to Save Report ISB52-04

Identification of key parameters for dispersion models

By

F Davies, C Collier, K Bozier & D Middleton.

Salford University and The Met Office

February 2003

Authorisation

Prepared by	Dr RI Young
Title	
Signature	
Date	February 2003
Location	QinetiQ Malvern

Principal authors	Professor C Collier
Appointment	Dean, Faculty of Science, Engineering & Environment.
Location	Salford University

Principal authors	Dr F Davies
Appointment	Research Fellow, ISB-52
Location	Salford University
Principal authors	Dr K Bozier
Appointment	Research Fellow, UFAM Instrumentation Scientist
Location	Salford University
Principal authors	Dr D R Middleton
Appointment	Air Quality Scientist
Location	Met Office, London

Record of changes

Issue	Date	Detail of Changes
0.1	8 October 2002	First Release
1.0	23 October 2002	More detailed explanation added to the data analysis
2.0	4 February 2003	Tables 5a & b added to summary
2.1	19 February 2003	Font corruption in Tables 5a & b corrected

Executive Summary ISB-52-04

This report ISB52-04 was produced under Project 52 of the Invest to Save Budget, or ISB. The aim of this project is to improve atmospheric pollution dispersion models with the goal of improving air quality forecasting. During the project life, the team will be developing a better understanding of airflow near the earth's surface, focussing especially on urban meteorology. This will be achieved through the gathering of accurate 3-Dimensional wind flow data using laser radar, also called lidar, and by incorporating that new knowledge into the dispersion models.

Lidar offers the ability to make some unique measurements within the urban environment that will be of great benefit to an improved understanding of pollution dispersal mechanisms within that environment. However care needs to be taken over deploying the lidars.

Earlier work has identified the flow field phenomena that it is important to observe in order to understand pollution dispersal mechanisms in the urban environment, the sampling scales necessary to accurately monitor these phenomena and suggested an experiment that deploys lidar to make the required observations.

In this report a demonstration is mad of how to derive the key parameters used by the various dispersion models from typical lidar observations. This starts with the measurement of wind and turbulence parameters from the line of sight lidar data**.** Calculations are then performed on this data to derive other meteorological parameters. Key amongst these are the kinetic energy dissipation rates and heat fluxes. Finally it is shown how the shape and height of the planetary boundary layer can be directly determined from the measurements.

The examples quoted are for observations taken by a single pulsed lidar system, the Salford one. However it should be noted that the data analysis techniques described herein are directly applicable to the resultant of combining observations from two pulsed lidars.

To summarise these findings two tables are presented which list the variables used in the Met Office NAME dispersion model, the dispersion model with which the Project Team is most familiar. Against these variables comments are made about whether the variable can be directly measured or inferred from the lidar data. It is clear from these comments that lidar has the ability to retrieve the pertinent spatial and temporal meteorological data required by dispersion models.

List of contents

1. INTRODUCTION

The aim of this Project is the improvement of air quality forecasting for the urban environment through the use of lidar data. Lidar offers the ability to make some unique measurements within the urban environment that will be of great benefit to an improved understanding of pollution dispersal mechanisms within that environment. However care needs to be taken over deploying the lidars.

For example lidar achieves measurements of high angular resolution through the use of a narrow beam divergence. The down side of this is that it takes a long time for the beam to scan over a large angular range. Therefore a lidar cannot monitor a complete wind field instantaneously; also data is produced by the lidar over an extended region. Current air quality models require point source information so there is a need to map the lidar observations to the inputs of the dispersion models. There is also the requirement to ensure the lidar observations are made on scales commensurate with the models.

The meteorological parameters used by the various dispersion models were listed in MS1 for further consideration, Middleton (01). Of these the most important to observe to understand pollution dispersal mechanisms are the shape of the planetary boundary layer (PBL) or mixing layer, and turbulence. The key flow parameters are mean flow, and turbulence. All dispersion models need these parameters described accurately. The currently existing models are well proven for the rural environment but would benefit from further adaptation for use in urban areas. In particular this implies a better description of the more complicated turbulence in the urban environment that is driven by the greater roughness scales that occur there.

The aim of the trials is to investigate how these quantities vary over the course of a day in both the rural and urban environments. In particular it will be important to observe the diurnal changes in turbulence and structure and depth of the mixing layer.

Possible ways to exploit this new knowledge within the models includes:

- identification of the appropriate update intervals for defining the properties of the mixing layer during the forecast calculation,
- providing a more appropriate description of the spatial variation across the mixing layer, including a more accurate description of the change in the height of the PBL at the rural urban interface,
- from an understanding of the differences in evolution of the mixing layer in the urban and rural environments, use separate models to reflect the differing temporal changes within the different environments,
- modelling of the turbulence to more accurately reflect the vertical thermal structure.

Earlier work has identified the flow field phenomena that it is important to observe in order to understand pollution dispersal mechanisms in the urban environment, the sampling scales necessary to accurately monitor these phenomena and suggested an experiment that deploys lidar to make the required observations, Young *et al* (02).

In this report a demonstration of how to derive the key parameters used by the various dispersion models from the lidar observations are made. The examples quoted are for observations taken by a single pulsed lidar system, the Salford one. However it should be noted that the data analysis techniques described herein are directly applicable to the resultant of combining observations from two pulsed lidars.

The Salford pulsed Doppler lidar has now been deployed using several scanning techniques to investigate wind flow and turbulence within the atmospheric boundary layer. Various techniques have been used to investigate both the temporal and spatial variability of the atmosphere and relevant meteorological parameters describing the atmosphere have been

calculated. Data from two field campaigns using the Salford pulsed Doppler infrared lidar system carried out in Greater Manchester are used in this analysis. These measurements are some of the first made using such an instrument in an urban area. The data were taken on 3rd April 2001 and 2rd - 7th May 2002. The second set of data was taken using the new upgraded system discussed in report ISB52-02.

2 CHARACTERISTICS OF THE SYSTEM

The Salford lidar system is based around the system described by Pearson and Collier (1999) although it has now been upgraded to use a Transverse Excitation Atmospheric (TEA) pressure laser. The characteristics of the previous and current systems are given in Table 1.

Parameters	Values	
	Old	New
Transmitter	CO_2 laser	CO_2 laser
Operating wavelength	10.6 μm	10.6 μm
Energy per pulse	0.7 mJ	70 mJ
Pulse repetition frequency (PRF)	120 Hz	upto 50Hz
Wind velocity accuracy	0.5 ms^{-1}	0.7 ms^{-1}
Range resolution	112 m	112 m
Maximum Range	4.6 km	10 km
Minimum Range	400 m	700 m

Table 1: Summary of the Salford lidar system parameters.

3 LIDAR SYSTEM PERFORMANCE

The derivation of turbulence variables depends upon the accurate estimation of wind velocity, momentum fluxes and distance. The lidar utilises backscattered power returns from distributed aerosols which de-correlate the return time series on time scales of the order of micro-seconds, although the returns from successive range gates and pulses are un-correlated. However, due to the larger Doppler shift at these wavelengths (at a wavelength of 10 μm the Doppler shift is approximately 200 KHz ms^{-1}), the return time series from a single pulse is sufficient for the Doppler analysis. The accumulation of the returns from multiple pulses is not a prerequisite for the Doppler analysis, but is a technique for performing speckle averaging and increasing the number of signal photo electrons per estimate, thereby obtaining improved Doppler and return power measurements. In the present system 50 pulses are usually averaged every second averaging less pulses reduces the maximum range.

The maximum range is a function of the signal to noise ratio (SNR) and the Doppler estimation procedure. The range resolution of the system is determined by both the pulse length and the number of points in the digitised time series used for each range gate in the signal processing. Using a high PRF, where the returns from multiple pulses can be incoherently accumulated over time scales in which atmospheric motion can be assumed to be constant (~ 1 s), is one way of achieving a compromise between range and Doppler resolution. Reducing the pulse length degrades the Doppler performance, which can be offset by the accumulation process. The error in line-of-sight velocity measurements using

the new lidar system are estimated as in Table 2 (see Section 5). For these calculations the signal was integrated over 80 pulses.

Range gate	SNR (db)	Error (m sec^{-1})
10 (1120 m)	10	0.7
40 (4480 m)	-5	1.0
60 (6720 m)	-14	1.1

Table 2: Errors in line-of-sight velocity estimates made using the new lidar

The system characteristics thus determine the rate at which data can be taken. In the data discussed in the following sections the old lidar system, which had a p.r.f. of 120 Hz and accumulated data over 120 pulses, recorded data at 1 Hz, while the new system, which had a p.r.f. set at 10 Hz and accumulated data over 50 pulses, recorded data at 0.2 Hz. The data record rate determines how fast the lidar beam can be scanned if we require good spatial resolution. With the new system a full azimuth scan (295°) took approximately 10 minutes while a full elevation scan (42°) took approximately 3 minutes.

4. DESCRIPTION OF FIELD CAMPAIGNS.

The measurements discussed in this report were gathered from two sites located near the University of Salford. Data from the observation days have been analysed and a summary is shown in Table 3. Here the Monin-Obukhov length, L, is used to characterise the stability conditions dominant on each day. The Monin-Obukhov stability length is defined as,

$$L = \left[\frac{-u_{*0}^{3}}{k(g/\overline{\theta}_v)\overline{w'\theta'}_v}\right] = -\left[\frac{u_{*0}^{2}}{k(g/\overline{\theta}_v)\theta_{v*0}}\right] \qquad (1)$$

Where θ_v = virtual potential temperature, u_{*0} = friction velocity , *k* = Von Karmon constant and g = acceleration due to gravity.

Where $\theta_{v*0} = \frac{\overline{w'\theta'_v}}{u_{*0}}$, $\overline{\theta_v}$ = layer mean virtual potential temperature, u_{*0} = friction velocity , *k* = Von Karmon constant and g = acceleration due to gravity.

Values of -z/L close to zero indicate neutral conditions with large positive values indicating increasing instability. Values of L for the cases discussed later were derived using the estimates of potential temperature - vertical velocity covariance (see Section 7) and friction velocity (see section 6) calculated from the lidar data, with a 2 m temperature measurement from the lidar van site.

The mean wind in table 3 is calculated using the procedure described in the following section.

Date	Measurement period (hours)	Mean wind at ~ 50m	- z/L	Weather type
3-4-01	1240 - 1530	6.4 ms^{-1} $\pm$ 0.2 ms^{-1}	0.23 (150m) 1.29 (250m)	Convective cloud developing; distant showers; 4/8ths cloud Cover
3-5-02	1000 - 1230	4.2 ms^{-1}	TBC	Convective with showers developing by mid-afternoon
7-5-02	1100 - 1330	8.4 ms^{-1}	TBC	Near Neutral with 8/8 cloud cover

Table 3: Case studies analysed

(-z/L is the stability parameter mentioned in report ISB51- MS01 section 5.10. In table 3 the number in brackets are the heights at which they were calculated.).

5 DERIVATION OF WIND AND TURBULENCE PROFILES

Retrieval of the mean wind components, $\overline{u}$, $\overline{v}$ and $\overline{w}$ from Doppler lidar data relied on the pointing or scanning geometry of the lidar beam. Using scanning methods, the mean wind components may be calculated by performing range height indicator (RHI, or elevation) scans or plan position indicator (PPI, or azimuth) scans. These enable radial wind velocities to be measured over an atmospheric volume. Following a method proposed by Gal-Chen *et al*. (1992) the mean wind, cross wind component, vertical velocity and associated momentum fluxes can be obtained from the radial (line of sight) wind velocity measurements. A PPI scan is carried out to determine the mean wind direction using VAD analysis (Browning and Wexler, 1968). This is followed by an RHI scan (0° - 42°) in the direction of the mean wind, where the vertical and the mean surface wind direction form a scan plane, *x* - *z*. An RHI scan is also performed at 90° to the mean wind direction where the vertical and the direction orthogonal to the mean surface wind forms a second scan plane, y - z. The sequence of RHI scans is performed continuously for a chosen time period. The data is divided into horizontal layers of a given depth, in this case 50 m thick with the lowest layer centred on a height of 50 m. The analysis of the data uses a least-square-fit statistical method to derive the relevant quantities. Since, in this method, the quantities are derived as mean layer values there is an implicit assumption that the wind field is homogeneous over the range of the lidar data. This also means that the calculated turbulence quantities are a measure of both the spatial and temporal variability of the atmosphere.

Davies *et al.* (2002) analysed the errors in the mean velocity estimates based on the Gal-Chen *et al* (1992) retrieval method using a simulated data set. Good estimates of the derived mean horizontal wind were found using this method up to heights of 2500m with errors of 0.24 ms^{-1}. The vertical velocity estimates were good between 500 - 2500 m with an error of 0.3 ms^{-1}. For low elevation angles (<10°) the vertical component of the radial wind is very small and the error on $\overline{w}$ increases.

An example of the $\overline{u}$, $\overline{v}$ and $\overline{w}$ profiles derived using this technique is shown in Figure 2a. Profiles derived from a sodar located on the edge of the urban area are 18 km away from the

lidar and measurements from a radiosonde launched some 120 km to the south-west are also shown for comparison.

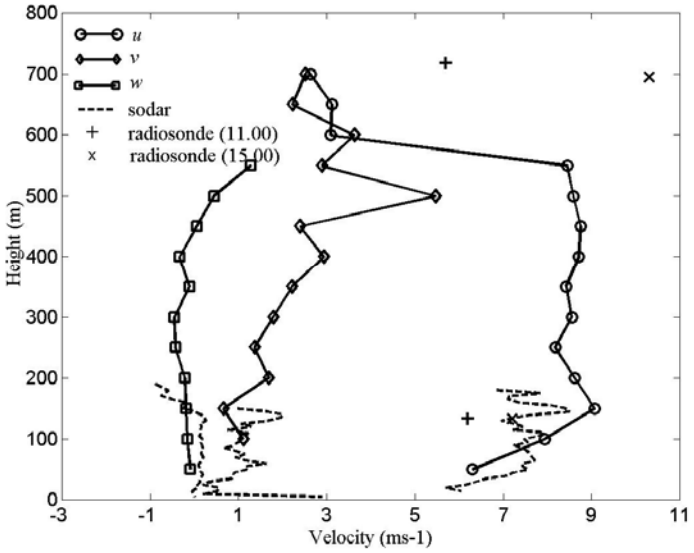

Figure 2a: *u, v* and *w* profiles derived from lidar data compared to sodar and radiosonde data for the 3rd April 2001.

The variance and turbulence parameters can also be calculated using the Gal-Chen (1992) technique. The vertical profiles of the variances of *u, v* and *w,* 1240 - 1530 hours on 3rd April 2001 are shown in Figure 2b. The figures in 2a, 2b and 3 were calculated using lidar data from the old lidar system. No comparison data was available for the turbulence parameters, but for the mean quantities the derived profiles compare well with the sodar data (figure 2a).

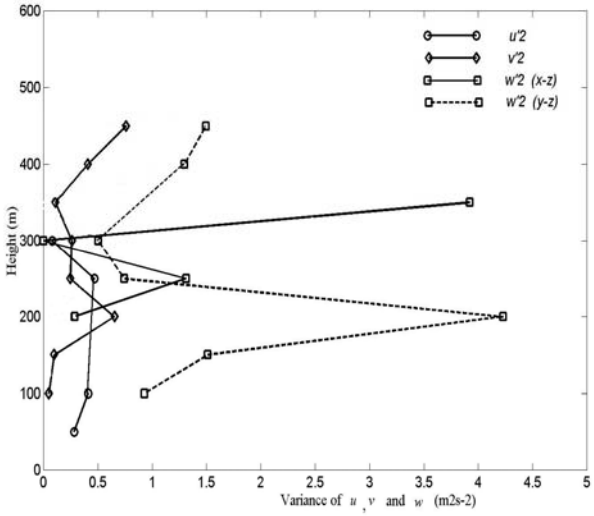

Figure 2b : Vertical profiles of the turbulence values derived from the lidar data

6 CALCULATIONS OF OTHER METEOROLOGICAL PARAMETERS

The vertical profiles of the momentum fluxes, $\overline{u'w'}$ and $\overline{v'w'}$, with height are shown in Figure 3 for the measurements made on 3rd April 2001 between 12.40 - 15.30 hours. The values of friction velocity, u_{*0}, calculated from equation (2).

$$u_{*0}^2 = \left[(u'w')_0^2 + (v'w')_0^2\right]^{\frac{1}{2}} \qquad (2)$$

This is evaluated for each height range, 50 - 300m as shown in Table 4.

Height, z (m)	Friction velocity, u_{*0} (ms^{-1})
50	0.41 $\pm$0.2
100	0.97 $\pm$ 0.2
150	1.28 $\pm$ 0.2
200	1.28 $\pm$ 0.3
250	0.93 $\pm$ 0.3
300	0.60 $\pm$ 0.4

Table 4: Friction velocity values, u_{*0} calculated from observations made between 12.40 and 15.30 for 3rd April 2001 case.

Within the constant flux layer (at a height of z_* to ~ 0.1 z_* where the z_* is the height of the roughness sub-layer, Roth 2000), the mean profiles obey logarithmic laws and Monin-Obukhov similarity theory applies. The height of the roughness sub-layer over this region is estimated to be 150 m, and the average value of the friction velocity over the height range 50-150m is u_{*0} = 0.89 ms^{-1}.

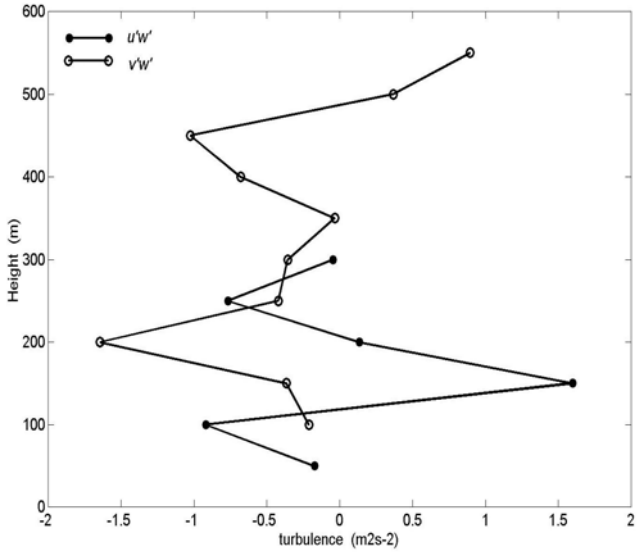

Figure 3 : Momentum flux values derived from lidar data on the 3rd April 2001.

The value of the drag coefficient has been evaluated for the height range 50-150m using equation (3) below.

$$C_D = \left(\frac{u_{*0}}{u} \right)^2 \qquad (3)$$

The drag coefficient varies over the height range, with a value of 0.43 x 10^{-2} occurring at 50m, for a wind speed of ~ 8 ms^{-1}. This value is reasonable compared to the values of the drag coefficient for medium height/high density surface elements, (0.9 x 10^{-2}) given by Grimmond and Oke (1999).

Since the atmospheric stability on 3rd April 2001 was determined as near neutral an estimate the roughness length, $z_{0,}$ can be calculated using equation (4).

$$\ln(z_0) = \ln z - k\left(\frac{u}{u_{*0}} \right) \qquad (4)$$

The value of ($\ln z - k\,5 / u_{*0}$) plotted in figure 4 can give an estimate of the roughness length, z_0. The profile of the mean wind over the height range 50 - 150m gives a value of z_0 of 4m.

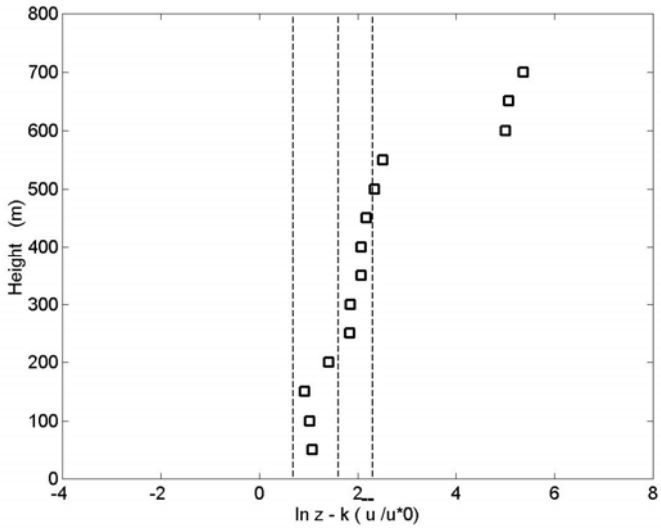

Figure 4 : Vertical profiles of ln z - *k* 5 / u_{*0} with height. The dashed lines mark roughness lengths of 2 m, 5 m and 10 m. Data collected 3rd April 2001.

Using the value of ~ 4m obtained from the measurements made on 3rd April 2001 and making comparisons with the tables of typical values given in Grimmond and Oke (1999), an estimate of z_0 = 0.7m is take for the aerodynamic roughness length, and z_d = 3.5m is obtained for the zero plane displacement. These values are comparable to those reported for Birmingham in the UK estimated from anemometer measurements reported by Rooney (2001).

The analysis above was done using data from the old lidar system. It was carried out primarily to look at the feasibility of using lidar data to derive urban roughness characteristic lengthscales. Since the Salford lidar system has been redesigned further development of this methodology is underway. This includes error analysis and corrections for various secondary signal processing considerations Davies (2003).

7 KINETIC ENERGY DISSIPATION AND HEAT FLUXES

Marht et al. (2001) analyse velocity variances collected at grassland, heather and forest sites, to determine the turbulent energy gap region for separating the turbulent and mesoscale motions in the data as discussed by Van der Hoven (1957). The mesoscale and turbulent motions seem most easily separated under stable conditions near the surface, and the choice of averaging time within the gap region does not affect calculation of the variances. The appropriate averaging period is between 0 - 100s for stable conditions, whilst for neutral conditions the gap region occurs between 10-1,000s. In the present work data were usually averaged over 300s.

The performance of the pulsed Doppler lidar in estimating the radial wind velocity is sufficient to enable estimates to be made of the spatial structure function, and consequently the kinetic energy dissipation (ε) of boundary layer. (for previous work see for example Frehlich et al., 1994, 1998; Hannon et al., 1995, Banakh et al., 1999. In the turbulent inertial range the expected power spectra relationship (see for example Batchelor, 1965) is given in equation 5.

$$\tilde{f}(k) = \alpha\varepsilon^{2/3}K^{-5/3} \qquad (5)$$

where *k* is the wave number, α is a universal constant and $\tilde{f}$ (*k*) is the Fourier transform of the longitudinal velocity correlation $\overline{u'(x)u'(x+r)}$ or $\overline{v'(y)v'(y+r)}$ where *u*' and v' are the fluctuations in the *u* and *v* velocities

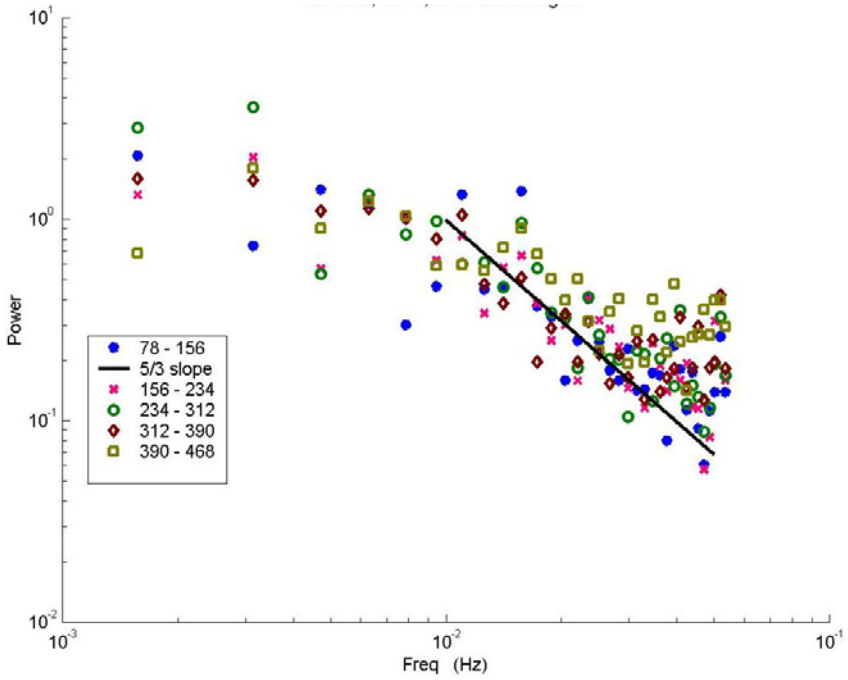

Figure 5 : Power spectrum of radial wind velocity taken at an elevation of 4 ° on 7th May 2002.

The kinetic energy dissipation may be estimated from the spectra provided that an inertial $k^{-5/3}$ law is established.). An example of the spectra derived on 7th May 2002 is shown in

Figure 5. The - 5/3 law fit straight line is superimposed upon the data in the figure. The kinetic energy dissipation rate derived using it gives, ε = 0.8 x 10^{-3} m^2 s^{-3}.

The balance of the vertical velocity fluctuations for horizontally homogenous turbulence is given by Wyngaard and Cote 1971;

$$\frac{\partial}{\partial z}\left(\frac{1}{2}\overline{w'^3}\right) = -\frac{1}{\rho_0}\left(w\frac{\partial \rho'}{\partial z}\right) - \frac{\varepsilon}{3} + \frac{g}{\theta_0}\overline{w'\theta'} \qquad (6)$$

where ρ' is the pressure fluctuation, ρ_0 is the air density at the surface, ε is the kinetic energy dissipation, *g* is the acceleration due to gravity, θ_0 is the potential temperature at the surface and θ' is the potential temperature perturbations. Wyngaard and Cote found that under unstable conditions (positive heat flux) the pressure term near the surface is small compared to the other terms, and can therefore be neglected. Hence, in the surface layer the heat flux can be estimated from the kinetic energy dissipation and the vertical gradient of the third moment of the vertical velocity. Since $\overline{w'\theta'}$ is the potential temperature-vertical velocity covariance then $\rho_0 C_p \overline{w'\theta'}$ is the surface heat flux, where C_p is the heat capacity of air at constant pressure. The vertical profiles of the momentum fluxes $\overline{u'w'}$ and $\overline{v'w'}$ are shown in Figure 3 for 3rd April 2001. The heat flux is estimated using the vertical profile of the third moment of the vertical velocity, $\overline{w'^3}$ at the lowest measurement level, and taking the kinetic energy dissipation rate above. Also taking $\frac{\theta_0}{g} = 30^0 s^2 m^{-1}$, then values of $\overline{w'\theta'}$ are obtained from the potential temperature-vertical velocity covariance. Using C_p = 1004 $jdeg^{-1}kg^{-1}$ and ρ_0 = 1.275 kgm^{-3} the surface heat flux values, $\rho_0 C_p \overline{w'\theta'}$, are evaluated as 99 Wm^{-2}.

8. SHAPE / HEIGHT OF PLANETARY BOUNDARY LAYER

The top of the atmospheric mixed layer can be measured using lidar intensity backscatter. This is discussed by Boers et al (1986), Dupont et al (1994), and Eilts et al (1985) . Lidar works by detecting the backscattered signal from aerosol particles in the atmosphere. Depending on the atmospheric conditions, these aerosol particles are trapped within the boundary layer below an inversion layer. The lidar therefore should give a clear signature of these trapped aerosols and therefore the height of this inversion layer. The lidar beam is however attenuated by the presence of water vapour. So the presence of diffuse cloud could possibly give large backscattered intensities throughout a measurable depth, whereas thick cloud would give a large signal at the cloud base and attenuate the beam beyond within a matter of metres (as in the data from 7th May 2002, figure 6 and 7).

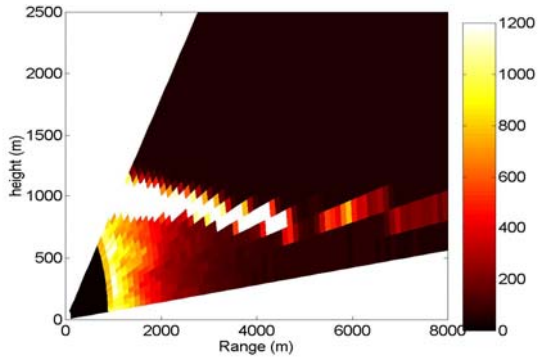

Figure 6 : Elevation (RHI) scan of signal intensity from 7th May 2002.

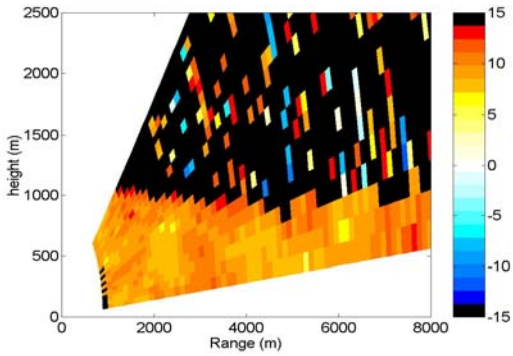

Figure 7 : As figure 6 but radial wind velocity.

Weather on the 3rd May 2002 was very convective. The sky started out clear and Cumulus were seen to build up during the day, and there were showers by mid afternoon.

Intensity and Velocity plots taken at 11:00 BST are shown in figures 8 and 9. In figure 8 no clear signature of the boundary layer top can be seen. The broken patchy signal could be interpreted as either diffuse cloud or 'dirty' air being lofted into the atmosphere above.

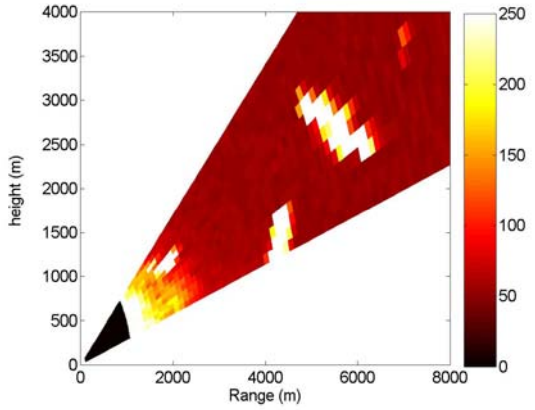

Figure 8 : Elevation scan of signal intensity for 3rd May 2002 .

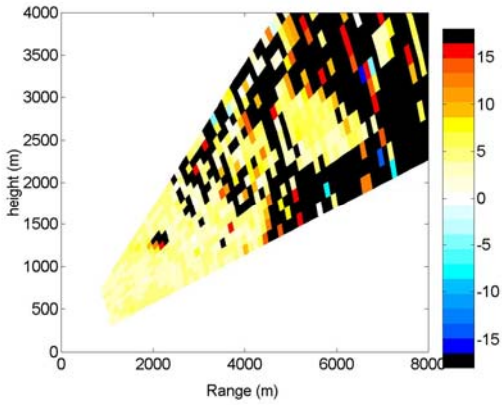

Figure 9 : As figure 8 but radial wind velocitv

A field trial has just been conducted (September 2002) where the Salford lidar was deployed along side the Met. Research Units' balloon and regular radiosondes. This data collected at Cardington will prove invaluable in defining the boundary layer top in comparison with the lidar data, as the location of the boundary layer top derived approximately from the radiosonde temperature will be available. It is intended to publish the results of this trial in Davies (2003).

9 SUMMARY

This report is the fourth milestone in the ISB Urban lidar project.

The contents of the report detail the deployment of the Salford lidar system under various atmospheric conditions. From these field campaigns lidar data has been used to calculate various wind and turbulence profiles, appropriate to pollution dispersal mechanisms. It is then demonstrated how the data can thereafter be used to calculate various other meteorological parameters. Due to the lidar scanning mechanism the lidar can be used to retrieve both spatial and temporal data. The potential of the lidar system to profile the top of the boundary layer has been demonstrated.

In summary tables 5a and 5b presents a revised list of the variables used in the Met Office NAME dispersion model. Table 5a places emphasis upon those variables that are measurable by lidar, or closely related to lidar quantities. Table 5b lists those parameters that cannot be measured by lidar or inferred from the measurements. For a full list of the variables from which this is derived see Table 3 of ISB52 Milestone 01 report by DR Middleton (2002).

Variable	Symbol	NAME Perspective	Lidar Perspective
Boundary layer depth	h	NAME has rural h value via UM NWP profiles. City has internal layer(s). Lidar to investigate height of lowest layer(s). Requires h at hourly steps for rural & urban. (Plume models require h.)	Strength of back-scatter signal identifies aerosol layer(s). Range & beam elevation give altitude. Scans could map urban/rural depths $h(x,y)$ to improve it in NAME.
Mean flow velocity (space or time average)	$\bar{u}$, $\bar{v}$, $\bar{w}$	NAME uses 3-D fields (UM NWP) of $\bar{u}$, $\bar{v}$, $\bar{w}$ updated each time-step. (Plume models use wind speed & wind direction at 10 m, and assume a wind profile, derivable from $\bar{u}$, $\bar{v}$, $\bar{w}$. 10m may be below beam.)	Lidars can be configured for instantaneous flow $u(z), v(z), w(z)$. Must measure repeatedly for sufficient sample. Processing to yield means $\bar{u}$, $\bar{v}$, $\bar{w}$ and fluctuations u', v', w' via $u' = u - \bar{u}$ etc.
Turbulence	σ_u, σ_v, σ_w	NAME uses standard deviations of wind velocity component fluctuations σ_u, σ_v, σ_w, as functions of position, altitude, stability & time. Calculated in NAME using h, L, w_*, u_*. (Plume models may use standard deviations of wind angles σ_θ, σ_ϕ)	Processing of fluctuations u', v', w' to obtain σ_u, σ_v, σ_w Turbulent kinetic energy of the fluctuations is then derived $TKE = \frac{1}{2}(\sigma_u^2 + \sigma_v^2 + \sigma_w^2)$ (σ_θ, σ_ϕ derivable from fluctuations u', v', w')
Local friction velocity derived from local Reynolds stress.	u_* $\overline{u'w'}$, $\overline{v'w'}$	NAME calculates u_* or uses UM NWP output for σ_u, σ_v, σ_w. For future development of NAME, any measured	Lidar processing yields Reynolds stress $\overline{u'w'}$, $\overline{v'w'}$ and friction velocity u_* via $u_*^2 = \left(\overline{u'w'}^2 + \overline{v'w'}^2\right)^{1/2}$.

		spatial changes in u_* are of great interest for urban roughness sub-layer. In future NAME may use profiles of $\overline{u'w'}$, $\overline{v'w'}$.	To examine lidar data for any evidence of spatial variation in u_*, $\overline{u'w'}$, $\overline{v'w'}$. Scanning in elevation sets minimum period & limits feasible number of scans
Log law for surface layer mean wind speed in neutral; modified using L in stable/unstable	$\bar{u} = \frac{u_*}{k}\ln\left(\frac{z-d}{z_0}\right)$ Notation: Use d or z_d.	NAME follows UM NWP log law with stability adjustment & velocity $\bar{u} \to 0$ at height $d + z_0$, when extrapolate profile to surface. NAME has displacement height $d = 0$. NAME has surface momentum roughness length $z_0(x, y)$ from data-base.	Lidar data for $\overline{u(z)}$ to verify profiles and check u_*, k, z_0, d. Usually von Karman constant $k \cong 0.4$ Lidar profile estimates of z_0 may be used to test urban morphology algorithms from the literature & check values in NAME.
Urban roughness sub-layer scale height	z_*	NAME may be extended to use z_* if urban roughness sub-layer confirmed. Height to which roughness affects turbulence statistics Height of maximum stress Mean building height $\bar{h}$ to be found from buildings' geometry to interpret results: $z_* \approx \beta\bar{h}$; $\beta \approx 1-5$. Need to establish β (if height of maximum stress detected in profile).	Lidar data for Reynolds stress and friction velocity may shed light on the existence of a stress maximum, for an urban roughness sub-layer, and its scaling height z_*. May not be detectable if lidar range height too high. Positive result will be valuable; null result inconclusive (hard to measure down near buildings).
Eddy dissipation rate	ε	NAME calculates ε for turbulence & plume rise schemes. Plume rise is important for fumigation by large stacks. No urban measurements are available for NAME. In inertial sub-range part of spectrum, $\ln F(\kappa_1)$ versus $\ln\kappa_1$ has intercept $\ln\left(\alpha_1\varepsilon^{2/3}\right)$. Kolmogorov constant is assumed $\alpha_1 \approx 0.5-0.6$	Lidar data on fluctuations processed to generate spectrum; measure intercept & estimate ε. Uses along-the-beam correlation of radial velocity. Scatter in data and 2/3 power may generate large uncertainty in ε value. May sample fixed beam elevation, analysing data in similar fashion to sonic data e.g. 10 minutes
Lagrangian integral timescale Lagrangian: sensing with the flow; very difficult to do.	$\tau_L = \int_0^\infty R(\tau)d\tau$	NAME uses τ_L in plume rise & turbulence schemes. No measurements to date are available for NAME. Calculated in NAME as separate horizontal & vertical scales.	Decay time scale for auto correlation coefficient $R(\tau) = \frac{\overline{u'(t)u'(t+\tau)}}{\sigma_u^2}$ for lag τ & velocity variance σ_u^2. Process lidar data for auto-correlation &

			integrate. At low elevation angle, using radial velocity as u.
Sensible heat flux Flux of temperature fluctuation (measurable by a sonic, but not lidar)	H or Q_H $H = Q_H = \rho C_p \overline{w'\theta'}$ $\overline{w'\theta'}$	Urban or rural heat carried up by convective eddies. Important to NAME for turbulence schemes: stability L depends on H and u_*. Since $u_* > 0$, sign of H determines sign of L. Correct sign of H (and time of transition) is very important for NAME.	Not directly from lidar as temperature fluctuations not measured. Indirectly from lidar third moment $\overline{w'^3}$ using Wyngaard & Cote (1971). Some doubts on accuracy of estimate of H via lidar data. Values of H, L rarely available for city. Vertical sensing of w' useful (perhaps with a shorter range lidar).
Monin Obukhov Length	$L = -\frac{\theta u_*^3 \rho C_p}{kgH}$	Key stability parameter in NAME. Stability scale height above which convection dominates turbulence.	Not directly from lidar. Indirectly from estimates of u_* and H.
Convective scaling velocity Associated with speed of convection (unstable)	$w_* = \left(hg \frac{\left(\overline{w'\theta'}\right)}{\theta} \right)^{1/3}$	Used in NAME for calculating turbulence, as $w_* = u_* \left(\frac{z_i}{k\lvert L\rvert} \right)^{1/3}$	Not directly from lidar, but the NAME formulation may be used (with $z_i = h$, and $k, \lvert L\rvert, u_*$ as above).

Table 5a. A <u>revised list</u> of variables used in Met Office NAME dispersion model, with emphasis upon those that are measurable by lidar, or closely related to lidar quantities. Time must refer to UTC (GMT). Met Office Unified Model is denoted by UM NWP.

Latent heat flux	λE or Q_E	Heat carried upwards by water vapour flux E and latent heat λ.	Not from lidar.
Ground heat flux	G or Q_S	Heat transfer flux into Ground G or Soil S	Not from lidar.
Building heat fluxes • From roofs • From walls		Analogous to G but into building fabric; plays role in urban heat store effect.	Not from lidar. (Scintillometers have been tried for optical remote sensing of heat fluxes over cities).
Anthropogenic heat flux		Released from energy use.	Not from lidar.
Solar radiation & long wave radiation • Trapping in canyons	R or Z, Q^*	After passage through cloud	Not from lidar.
Precipitation		For wetness of surface	Not from lidar.
Temperature above and just below ground level.	$\theta(z)$ or $T(z)$	Sensor response: Lapse rate: slow. Sensible heat flux: fast. Ground: slow.	Not from lidar.
Potential Temperature	$\theta(z)$	NAME plume rise as well as plume models use the lapse rate $\frac{\partial\theta}{\partial z}$	Not from lidar.
Mean temperature	$\overline{\theta}$	Batch/running mean of θ	Not from lidar.
Temperature fluctuation	θ'	From $\theta' = \theta - \overline{\theta}$, usually via sonic or fast thermometer	Not from lidar.
Brunt Vaisala frequency (stable lapse rate)	$N = \sqrt{\left(\frac{g}{\theta_e}\right)\left(\frac{\partial\theta_e}{\partial z}\right)}$	Associated with buoyancy restoring force (stable lapse rate)	Not from lidar.

Table 5b. A <u>revised list</u> of other variables used in Met Office NAME dispersion model, that are not likely to be measurable by lidar.

9 REFERENCES

Banakh, V.A., Smalilikho, I.N., Kopp, F. and Verner, C. (1999) " Measurements of turbulence energy dissipation rate with a CW Doppler lidar in the atmospheric boundary layer, "J.Atm. Ocean. Tech., 16, 1044-1061.

Batchelor, G.K. (1965) The theory of homogeneous turbulence, Cambridge Univ., Press., New York 197pp.

Boers R. and Eloranta E.W. (1986) ' Lidar measurements of the atmospheric entrainment zone and the potential temperature jump across the top of the mixed layer.' Boundary Layer Meterology, 34, 357 - 375

Browning, K.A. and Wexler R. (1968) "The determination of kinetic properties of a wind field using Doppler radar, "J. App. Met., 7, 105-113.

Davies et al, “Comparison of wind and turbulence data from a pulsed Doppler lidar system, A UHF wind profiler and a tethered balloon”, submitted to Journal Applied Meteorology

Davies, F., Collier, C.G., Bozier, K.E. and Pearson, G.N. (2002) "On the accuracy of retrieved wind information from Doppler lidar observations", to appear in Quart. J.R. Met. Soc.

Dupont E. ,Pelon J. and Flamant C. (1994) 'Study of the moist convective boundary layer structure by backscattering lidar.' Boundary layer Meterorology, 69, 1 -26

Eilts, M.D., Sundararajan A. and Doviak R.J. (1985) ' The structure of the atmospheric boundary layer as revealed by lidar and Doppler radars'. Boundary Layer Meteorology, 31, 109 - 125

Frehlich, R.G., Hannon, S.M. and Henderson, S.W. 1994 'Performance of a 2 μm coherent Doppler lidar for wind measurements', J. Atmos. Ocean Tech., 11, 1517-1528.

Frehlich, R.G., Hannon, S.M. and Henderson, S.W. 1998 'Coherent Doppler lidar measurements of wind field statistics', Boundary-Layer Met., 86, 233-256.

Gal Chen, T., Xu, M. and Eberhard, W.L. (1992) "Estimations of atmospheric boundary layer fluxes and other turbulence parameters from Doppler lidar data", J. Geophys. Res., 97, D17, 18409 - 18423.

Grimmond, C.S.B. and Oke, T.R.: 1999, 'Aerodynamic properties of urban areas derived from analysis of surface form', J. App. Met., 38, 1262 - 1292.

Hannon, S.M., Thomson, J.A.L., Henderson, S.W. and Huffacker, R.M. 1995 `Windshear, turbulence and wake vortex characterisation using pulsed solid-state coherent lidar', Air Traffic Control Tech. Proc. SPIE, 2564 94-102.

Mahrt, L., Moore, E. and Vickers, D.: 2001, 'Dependence of turbulent and mesoscale velocity variances on scale and stability', J. App. Met., 40, 628-641.

Middleton D. Matching urban lidar data to dispersion models. ISB52-01. March 02.

Pearson, G.N. and Collier, C.G.: 1999, 'A pulsed coherent CO_2 lidar for boundary-layer meteorology', Quart. J.R. Met. Soc., 125, 2703 - 2721.

Pearson, GN DV Willetts & RI Young. Boundary layer meteorology by pulsed lidar. ISB52-02. April 02.

Rooney, G.G.: 2001, 'Comparison of upwind land use and roughness length measured in the urban boundary layer', Boundary-Layer Met., 100, 469-486.

Roth, M. :2000, 'Review of turbulence over cities'. Quart. J.R. Met. Soc. 126, 941-990

Rye, B.J. and Frehlich, R.G. 1991, 'The truncated Gaussian lidar antenna problems revisited', Paper WA6 in Tech. Digest on Coherent Laser Radar: Tech & Apps., Optical Soc. AM., Washington D.C.

Van der Hoven, I. 1957 'Power Spectrum of horizontal wind speed in the frequency range from 0.0007 to 900 cycles per hour', J. App. Met., 14, 160.

Wynggard, J.C. and Cote, O.R.: 1971, 'The budgets of turbulence kinetic energy and temperature variance in the atmospheric surface layer', J.Atmos. Sci., 28, 190-201.

Young RI, S Siemen, AR Holt & GJG Upton. Identification of key flow parameters for visualisation. ISB52-03 Aug 02.

11 GLOSSARY

K Von Karmon constant

PBL Planetary Boundary Layer

RHI Range Height Indicator

PRF Pulse Repetition Frequency

PPI Plan Position Indicator

VAD Velocity Azimuth Display

z0 is the aerodynamic roughness length which is an integration constant such that the logarithmic wind profile extrapolates to zero at z=z0. This is discussed in report ISB51 -01, section 5.2

zd is the displacement height, i.e. the level between the top and bottom of the roughness elements above which the logarithmic profile applies.

12 ACKNOWLEDGEMENTS

This work was funded by HM Treasury under the Invest to Save Budget. Department for Environment, Food and Rural Affairs (DEFRA) acted on behalf of HM Treasury. QinetiQ work described herein was supported under Contract Number CU016-0000014438 and this support is acknowledged. The authors also acknowledge assistance from members of the Urban Lidar Project (Met Office, University of Essex and QinetiQ). The authors also wish to acknowledge the assistance given by David Thomson in the preparation of Table 5.

13 DISCLAIMER

14 DISTRIBUTION LIST

Copy No.	Name	Address
1-4	Dr Janet Dixon	DEFRA
5	Prof D V Willetts	PD315, QinetiQ Malvern
6	Dr G N Pearson	PD313, QinetiQ Malvern
7	Dr R I Young	PD115, QinetiQ Malvern
8-11	Dr D Middleton	Met Office, London
12	Prof C Collier	Salford University
13	Dr F Davies	Salford University
14	Dr K Bozier	Salford University
15	Prof A Holt	Essex University
16	Dr G Upton	Essex University
17	Dr S Siemen	Essex University
18	Project File	PD115, QinetiQ Malvern
19-23	Spares	PD115, QinetiQ Malvern